coatings

MDPI

Article

Magnetron Sputtering of Au-Based Alloys on NiTi Elements: Surface Investigation for New Products in SMA-Based Fashion and Luxury Accessories and Watchmaking

Francesca Villa [1,2,*], Enrico Bassani [1], Francesca Passaretti [1], Giuseppe de Ceglia [3], Stefano Viscuso [4], Valentina Zin [5], Enrico Miorin [5], Silvia Maria Deambrosis [5] and Elena Villa [1]

1 Institute of Condensed Matter Chemistry and Technologies for Energy-National Research Council (CNR-ICMATE) Lecco Unit, Via G. Previati, 1/E, 23900 Lecco, LC, Italy; enrico.bassani@cnr.it (E.B.); francesca.passaretti@cnr.it (F.P.); elena.villa@cnr.it (E.V.)
2 Mechanical Department, Politecnico di Milano, Via La Masa, 1, 20156 Milano, MI, Italy
3 Technosprings Italia Srl, Via G. Puccini, 4, 21010 Besnate, VA, Italy; g.deceglia@technosprings.com
4 TSS Innovations Projekte GmbH, Via Cantonale, 6535 Roveredo, GR, Switzerland; tss.en@tss-innovationsprojekte.ch
5 Institute of Condensed Matter Chemistry and Technologies for Energy-National Research Council (CNR-ICMATE) Padova Unit, C.so Stati Uniti, 4, 35127 Padova, PD, Italy; valentina.zin@cnr.it (V.Z.); enrico.miorin@cnr.it (E.M.); silviamaria.deambrosis@cnr.it (S.M.D.)
* Correspondence: francesca.villa@icmate.cnr.it

Abstract: A novel approach for the deposition of Au-based coatings on NiTi components was proposed to give rise to innovative SMA-based products for the fashion, luxury, and watchmaking fields. Different Au-Cu and Au-Ag-Cu alloys (with confidential compositions within the color designations 2N, 4N, and 5N) were deposited by magnetron sputtering on superelastic and shape-memory NiTi ribbons. After preliminary morphological and microstructural characterizations, the influence of the film deposition on the functional, mechanical, and tribological behavior was deeply investigated. The macroscopic mechanical properties, including the damping, superelastic, and shape recovery characteristics, were not affected since the behavior upon both small and severe deformations was unchanged and the coatings were not damaged. Indeed, both the film adhesion and the precious aspect were maintained. Furthermore, a more detailed surface characterization, through nanoindentation, tribocorrosion, and scratch and wear tests, was performed. This experimental investigation evidenced the ductile behavior of the Au-based films and their good adhesion on NiTi substrates. Moreover, the coatings exhibited a good wear resistance, both in dry conditions and simulated body fluids, which proved to be suitable for fashion and watchmaking fields. Despite slight differences being observed within the films' responses, all of them could be considered suitable and interesting for the design of smart luxury accessories, proving that the chosen deposition process is sound and reliable for these applications.

Keywords: NiTi; shape-memory alloys; magnetron sputtering; Au-based coatings; mechanical properties; wear; tribocorrosion; watchmaking; gold alloys

check for updates

Citation: Villa, F.; Bassani, E.; Passaretti, F.; de Ceglia, G.; Viscuso, S.; Zin, V.; Miorin, E.; Deambrosis, S.M.; Villa, E. Magnetron Sputtering of Au-Based Alloys on NiTi Elements: Surface Investigation for New Products in SMA-Based Fashion and Luxury Accessories and Watchmaking. *Coatings* **2022**, *12*, 136. https://doi.org/10.3390/coatings12020136

Academic Editor: Jeff Rao

Received: 16 December 2021
Accepted: 18 January 2022
Published: 24 January 2022

Publisher's Note: MDPI stays neutral with regard to jurisdictional claims in published maps and institutional affiliations.

Copyright: © 2022 by the authors. Licensee MDPI, Basel, Switzerland. This article is an open access article distributed under the terms and conditions of the Creative Commons Attribution (CC BY) license (https://creativecommons.org/licenses/by/4.0/).

1. Introduction

NiTi and derived ternary alloys are well-known functional materials that belong to the shape-memory alloys (SMAs) family and allow to develop innovative solutions related to their shape memory and superelastic properties [1,2]. Thanks to these functional features, different applications were proposed in industrial and biomedical fields, including thermo-mechanical actuation devices, structural damping solutions, and various biomedical products, e.g., orthodontic wires and stents. Moreover, the use of NiTi alloys is increasing also in other unusual sectors, with particular attention to watchmaking as well as the high luxury and fashion markets.

For the last two applications mentioned above, some examples of SMA exploitation were presented in the literature in recent years. Above all, the development of novel, precious Au-based alloys, such as Spangold [3,4], were introduced, and the principal effect that was exploited is the coloring and the peculiar artistic surface supplied by the martensitic structure. In addition to the widely studied Spangold and Au-Cu-based systems, NiTiAu was also considered and studied as a precious alloy with high-temperature SMA behavior [5–7]. In this case, both the microstructural condition and the improvement of functional properties were investigated, however, no specific products were implemented. On the other hand, NiTi elements including wires, ribbons, or small plates were patented for their application as interior supports or closures for bracelets, necklaces, rings, and other accessories to exploit the superelasticity or shape recovery properties in the final products [8–13]. In this case, given that the fashion sector requires necessary aesthetic requirements to be met, it is necessary to coat the NiTi alloy with coatings that have both design and protective purposes.

In the present study, we considered the possibility of opening a new perspective for the luxury and fashion markets. A new set of innovative accessories could be developed based on the unique functional characteristics of the SMA in combination with an improved aesthetic and intrinsic value of the ornament. This may be achieved through the deposition of Au-based alloy films, designed for decorative applications to approach the different gold color standards (1N, 2N, etc.) [14]. This could provide more freedom in components' shape and size and designing more compact and novel products with a global functional response of the whole device. Indeed, following this approach, the precious element of the whole accessory could be the coated SMA element, without having two distinct structures but a single "hybrid" component instead. This could result also in economic benefits, since the content of precious alloys is lower in the case of coated elements than in the presence of precious bulky components.

Considering Au-based coatings, different kinds of deposition technologies were implemented and proposed in the literature, including electrodeposition or chemical/physical vapor deposition. Coatings are commonly applied in machining tools due to their high hardness and wear-resistance, but they also can be exploited in the fashion field for decorative purposes. So far, the deposition of Au-based alloys on SMA substrates, in particular, NiTi, was studied almost exclusively for applications in the biomedical field. The Au element deposition was investigated also in combination with other materials like Rh, Ir, or polymers [15–17]. The main aim of these processes is dual: first, the deposited films increase the biocompatibility of the biomedical device for vascular, orthopedic, or orthodontic applications by reducing the Nickel release and improving antibacterial function of the device's surface. Second, the coatings improve the corrosion resistance of surfaces exposed to body fluids [18–22].

Lately, several variants were developed around the main deposition techniques: arc evaporation and sputtering. Considering the jewelry sector, the coating thickness required to produce satisfactory mechanical properties is below 1 μm. The increase in surface layer hardness is a desirable effect, typical of PVD products [23,24], which makes up for the very low thickness compared to that of electroplating (5–10 μm) [25]. The main advantages of magnetron sputtering over conventional electroplating are that it is a nonpolluting process that produces highly adherent coatings with high optical, electrical, and nonporous qualities, even when they are less than 1 μm in thickness [26]. However, some weaknesses of the magnetron sputtering technique concern the poor uniformity of the film thickness and the difficult coverage of substrates with complex geometries.

We investigated PVD magnetron-sputtering deposition of Au-based alloys on NiTi substrates with the aim of preliminarily exploring the quality and protective action of deposited thin films in dry and simulated human body environments. The effects of the deposition process on NiTi functional properties were studied by thermo-mechanical analysis and dynamic mechanical measurements. The surface quality was examined by a complete microscopy observation. In addition, the surface mechanical properties, film/substrate

adhesion, and tribocorrosion behavior of the coated samples were deeply investigated. These characterizations could provide an interesting overview of the performance and suitability of these novel products for the design of innovative fashion and luxury accessories. The novelty and the academic contribution are that the present work fills the gap in the literature related to magnetron sputtering of Au-based alloys on NiTi substrates through extensive and exhaustive surface characterizations. In addition, it provides inspiration for the extension of the use of the Au-coated elements in the growing fashion and watchmaking sectors and not only the specific and demanding biomedical field.

2. Materials and Methods

2.1. Deposition Process

Two NiTi elements with dimensions of 50 × 4 × 0.5 and 50 × 4 × 1.1 mm^3, respectively, were coated with different Au-based alloys via magneton sputtering. First, the NiTi components were cleaned in an automated cleaning line with alkaline detergents in ultrasonic baths, followed by hot air drying. In the magnetron sputtering system, the components' surfaces were activated with argon plasma in radio-frequency (RF) mode. The duration of this activation step was 10 min, with an argon pressure of 0.01 mbar and an RF power of 800 W. To improve the coating adhesion, an 80 nm-thick titanium glue layer was grown through sputtering of a pure titanium target in direct current (DC) mode for 5 min in a pure argon atmosphere. The final step of the process was the deposition of the gold-alloy layer with a thickness of 300 nm. Three different gold-alloy targets, i.e., 2N, 4N, and 5N, according to [14], were sputtered on the NiTi substrates. The gold-alloys contained a variable proportion of gold, silver, and copper, while preserving a gold weight percentage of over 750/1000. The resulting different finishes are shown in Figure 1. More specific details concerning the deposition process and the alloys' compositions cannot be shared since they are subject to industrial confidentiality.

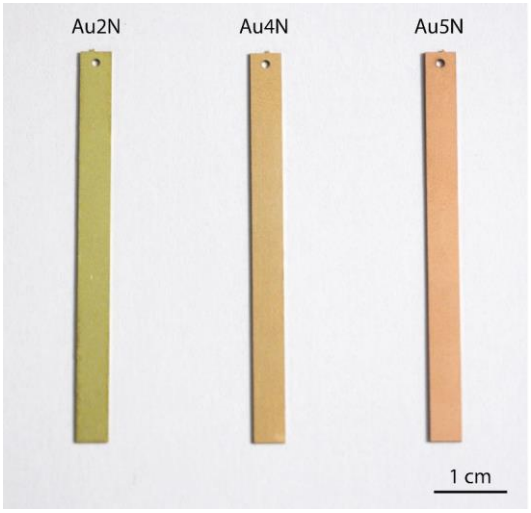

Figure 1. Au-coated NiTi elements.

2.2. Morphological and Microstructural Analysis and Characterization of Functional Properties

The compositional analyses were conducted by means of a Scanning Electron Microscope (SEM) LEO 1430 (Zeiss, Oberkochen, Germany) equipped with an INCA Energy 200 dispersive X-Ray Spectroscopy (EDS) probe (Oxford Instruments, Abingdon-on-Thames, UK). Moreover, a direct observation of the morphology of the coatings, before and after the mechanical tests, was performed through Leitz-ARISTOMET optical microscope (Leica Microsystems, Wetzlar, Germany) and SEM LEO 1430 microscope. X-ray diffraction (XRD) analyses were conducted using an X-Ray Diffractometer Panalytical XPert PRO (Malvern Panalytical, Malvern, UK) at 150 °C. The characterization of the functional properties of coated and uncoated NiTi elements was provided by the calorimetric analysis and the me-

chanical tests, including dynamic mechanical thermal analysis (DMTA), cyclic stress-strain measurements, and free shape recovery tests. The calorimetry analysis was conducted through the differential scanning calorimetry (DSC) Q200 (TA Instruments, New Castle, DE, USA), equipped with an LNCS cooling system (TA Instruments, New Castle, DE, USA), between −100 and 150 °C with a rate of 10 °C/min. The evaluation of the damping behavior of the NiTi elements was performed by means of DMTA on a dynamic mechanical analyzer Q800 (TA Instruments, New Castle, DE, USA) equipped with a GCA cooling system (TA Instruments, New Castle, DE, USA). The samples were subjected to a sinusoidal strain in the order of 10^{-4} in three-point-bending configuration under temperature variation (2 °C/min). Moreover, 1000 loading–unloading cycles were performed on the samples in three-point-bending configuration at constant temperatures (80 and 130 °C for 0.5 mm- and 1.1 mm-thick samples, respectively) and a frequency (1 Hz) up to an imposed strain of approximately 1% with the Instron E3000 instrument (Instron, Norwood, MA, USA), equipped with a thermal chamber. Finally, some free shape recovery tests were conducted on the coated samples involving a u-shape folding at low temperatures (approximately −20 °C, under gaseous nitrogen flow) and a subsequent heating up to high temperatures (approximately 200 °C, on a hotplate). The effects of the mechanical tests on the integrity and morphology of the coatings were evaluated by means of direct observation through optical and SEM microscopy right after the tests.

2.3. Mechanical Properties of the Coatings

The tests for the determination of mechanical properties, adhesion, wear, and tribocorrosion resistance were performed on the films deposited on the thickest substrates to allow better stability and reliability of the measurements. Surface topography measurements were performed by contact profilometry (DektakXT Stylus Profiler, Bruker) (Bruker Nano GmbH, Karlsruhe, Germany). Mechanical properties of the coatings, i.e., hardness (H) and elastic modulus (E), were measured by instrumented indentation testing (NanoTest, Micro Materials) (Micro Materials, Wrexham, UK) equipped with a Berkovich diamond tip (Micro Materials, Wrexham, UK), with a face angle of 142.3° (elastic modulus E = 1140 GPa, and Poisson ratio ν = 0.07). The indenter shape was calibrated using a series of indentation procedures in a fused silica standard between 0.5 and 200 mN. The easiest way to measure a hardness depth profile, with no additional sample preparation, is to apply increasing loads in the direction perpendicular to the surface. Continuous Multicycle (CMC)—or load-partial unload testing—was used, recording continuously both the indenter load and displacement. The Oliver and Pharr method [27,28] was applied at the resultant load—displacement curves. For each indentation, 20 cycles were performed up to a depth of 300 nm. In this kind of test, the indentation is carried out by a successive cycle of loading and partial unloading with a progressively increasing peak load, or equivalently, an increasing max depth of penetration. During partial unloading, the indenter is still in contact with the indented sample and the minimum load can be held for a predefined time. In the last cycle, unloading is complete. By applying elastic contact mechanics concepts, any of the obtained unloading curves can be correlated with the elastic properties of the indented material. This procedure allows to determine the effective hardness and modulus as a function of depth. Consistent with the Oliver and Pharr method applied to the single loading and unloading curve, the key quantities identified from this analysis are the contact area at full loading and the corresponding contact stiffness, leading to the determination of hardness and elastic modulus, respectively.

To investigate the adhesion and delamination resistance of Au-based coatings, scratch tests were also executed, and they were also employed to study the failure mechanisms of the films and of the film/substrate interface. The experiments were carried out using a diamond Rockwell tip (Bruker Nano GmbH, Karlsruhe, Germany); the maximum load of the diamond tip was 50 N, and the scratch length was set to apply load with a constant rate of 100 N/min, moving the sample at 10 mm/min, according to ISO 20502 [29]. To ensure

that we produced reliable data, the scratch test was repeated on each coating surface three times. The scratch tracks were then observed using a SEM.

Dry sliding wear tests were carried out according to the ASTM: G133-05 [30] on an oscillating friction and wear tester (UMT-2, Cetr) (Center for Tribology (CETR), Campbell, CA, USA) set for pure sliding contact. Ball-on-flat geometry was chosen for the sliding tests, with the aim of reaching high Hertzian contact pressure on coupled surfaces through a nonconformal contact type [31]. The counterparts were 5 mm diameter 100Cr6 stainless steel. An initial Hertzian contact pressure of 500 MPa was set, and a 2 mm stroke in linear reciprocating motion mode was applied with a frequency of 2 Hz. Tests lasted for 1000 back-and-forth cycles to avoid the complete removal of the coatings from the NiTi substrates, thus leading to the investigation of the wear mode in test conditions. To guarantee the reproducibility of the results, four tests with the same parameters were performed on each sample. Although the curves obtained for the friction coefficients as a function of sliding cycle number did not exactly overlap, the trends were similar.

2.4. Tribocorrosion Characterization

Tribocorrosion characterization was carried out in simulated seawater. For tests, 5 mm diameter ZrO_2 insulating balls were used as counterparts, and ball-on-flat configuration was set like wear tests in dry conditions. Tribocorrosion experiments were performed in a three-electrode cell, using an $Ag/AgCl/KCl_{sat}$ electrode as reference, a platinum wire as counter electrode, and the sample (film + substrate) as working electrode. Physiological Ringer's solution was selected as electrolyte, which was kept at a controlled temperature, simulating the human body fluid and composed as follows: 9 g/L NaCl, 0.43 g/L KCl, 0.2 g/L $NaHCO_3$, 0.24 g/L $CaCl_2$, according to the literature [32,33]. The tribocorrosion test under open cell voltage (*OCV*) condition was divided into three stages, including soaking, sliding, and passivation. Each sample was first immersed in the Ringer's solution (100 mL) at (37 ± 1) °C for 30 min to reach a stable open circuit potential. Then, sliding phase was carried out, which lasted for 30 min at a frequency of 2 Hz for a stroke of 2 mm. The normal load was kept constant to obtain 200 MPa of initial Hertzian contact pressure. The *OCV* and friction coefficient evolutions were continuously recorded for all the sliding time. When the sliding friction was stopped, *OCV* was recorded for 30 min again to evaluate the passivation behaviors of NiTi and coating surface. After that, the wear tracks of NiTi and Au-Cu-Ag coatings were observed and analyzed using FE-SEM (Sigma Zeiss) (Zeiss, Oberkochen, Germany) equipped with energy dispersive electron probe microanalyses (EDS, Oxford X-Max) (Oxford Instruments, Abingdon-on-Thames, UK). All the tribocorrosion tests were conducted at least twice to confirm the repeatability.

3. Results and Discussion

3.1. Morphological, Compositional, and Microstructural Characterization

The surface morphology of the three different Au-based films was observed through optical microscope, and an example is reported in Figure 2. The surface did not appear completely smooth, since the film was deposited on a substrate that exhibited an irregular topology and a mean roughness of Ra = 0.5 µm. This inhomogeneity could be ascribed to the production process of the NiTi substrate itself, which involved lamination and pickling.

Coating surfaces appear with a rough morphology, consisting of many clusters or agglomerates of small granules. Generally, magnetron sputtering processes lead to the growth of strongly columnar coatings with high residual stress levels [34]. Obtained thin film systems in general suffer from an inherent lack of ductility.

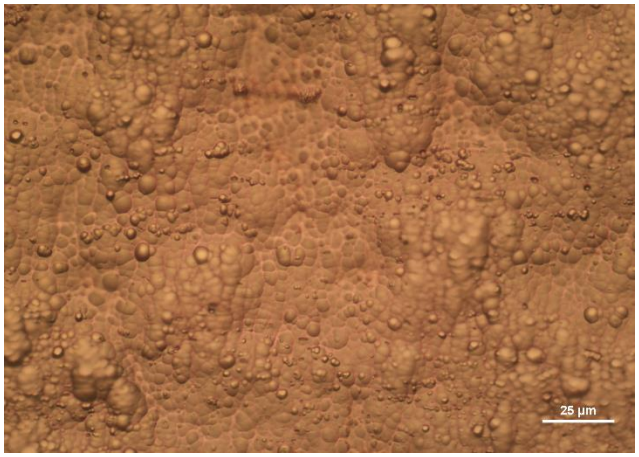

Figure 2. Optical micrograph of Au5N coating.

However, magnetron sputtering parameters can be combined with tailored chemical compositions and microstructures in final products. Equiaxed grains represent a decisive advantage to accommodate major deformation in grain-boundary incorporated processes, such as grain-boundary sliding due to the application of external stress and inducing deformation for which columnar grains would not be adequate because of their microstructural brittleness [35].

The composition of the films provided by the energy-dispersive X-ray spectroscopy (X-EDS) analysis and the resulting different colorations are in accordance with the indication given by the standards [14]. Au2N and Au4N are composed by Au-Cu-Ag alloys with approximately the same Au content and a different Cu/Ag ratio, while Au5N is a silver-free Au-Cu alloy. Increasing the Cu content subsequently increases the reddish coloring, as could be observed in Figure 1: the colorations are light yellow, pink, and red for Au2N, Au4N, and Au5N, respectively.

XRD measurements allow for the investigation of the microstructure of deposited Au-based coatings, as shown in Figure 3.

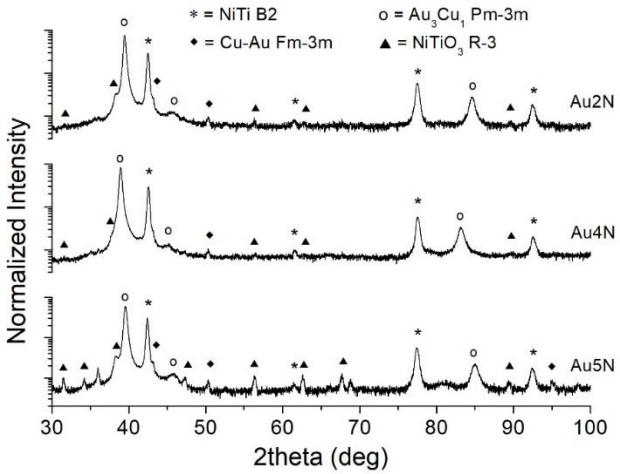

Figure 3. X-ray diffraction (XRD) spectra of deposited Au-based coatings.

The room temperature equilibrium phase diagram of Au-Cu-Ag is currently not well understood. However, several Au-Cu intermediate phases (e.g., Au_3Cu, AuCu, $AuCu_3$) are predicted to exist, depending on the Cu concentrations. Moreover, a wide range of metastable supersaturated solid solutions can appear with the use of nonequilibrium synthesis process, such as magnetron sputtering [36]. Ag, due to its complete miscibility with gold, tends to substitute it within crystal lattice.

Collected spectra revealed the coexistence of two phases: (i) a cubic intermetallic compound of Au_3Cu-type (Pm-3m) and (ii) a face-centered (Fm-3m) cubic solid solution [37]. No significant variations in the speculated crystal structures were observed among the three films. All samples exhibited strong 111 fiber texture. Signals from substrate oxidation, mainly in sample Au5N, were detected, coming from the underlying substrate [38]. Other peaks belong to the NiTi B2 cubic structure, which is typical of such shape-memory alloys.

Due to the microstructural uniformity of three deposited Au-based coatings, no significant variations in mechanical and tribological behavior of these materials would be expected during functional characterization.

3.2. Characterization of the Functional Properties

The calorimetric analysis through DSC (Figure 4) allowed the characterization of the functional transition of the two NiTi substrates through the evaluation of the characteristic temperatures and enthalpies of the thermoelastic martensitic transformation (TMT), which are reported in Table 1. M_s and M_f are the temperatures corresponding to the beginning and the end, respectively, of the martensitic transformation upon cooling from the parent austenitic phase, which is stable at high temperatures, and the martensitic phase, at low temperatures. In this case, the transformation is the direct TMT, and ΔH_{heat} is the energy involved in this first-order transition. Conversely, A_s, A_f, and ΔH_{cool} are the characteristic parameters of the inverse TMT, which occurs upon heating.

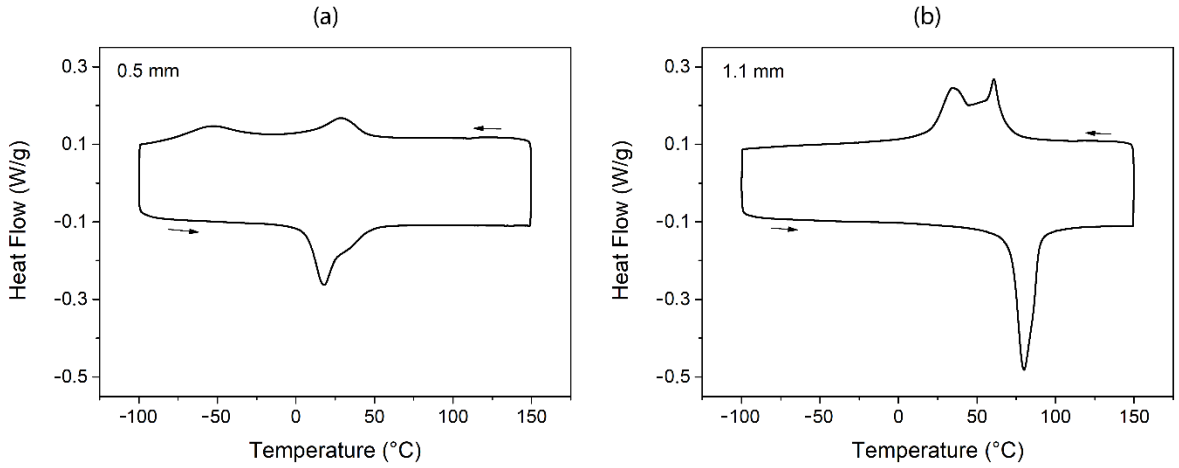

Figure 4. Differential scanning calorimetry (DSC) analysis for samples with thickness of 0.5 mm (**a**) and 1.1 mm (**b**).

Table 1. Transformation temperatures and enthalpies for the two NiTi substrates.

Sample	M_s (°C)	M_f (°C)	A_s (°C)	A_f (°C)	ΔH_{cool} (J/g)	ΔH_{heat} (J/g)
NiTi 0.5	46.3	−81.4	5.9	48.3	23.5	21.7
NiTi 1.1	73.0	19.7	71.3	90.7	33.4	32.9

The TMT occurs above room temperature in the case of the 0.5mm-thick NiTi element, which could be classified as a shape-memory material, while the thinner element transforms below room temperature; hence, around this temperature it could be considered a superelastic alloy. In both cases, the DSC curves in the cooling stage present a well-defined double peak, revealing a two-step martensitic transition.

The effects of the Au-based films on the functional properties, i.e., pseudoelasticity, damping, and shape-memory ability of NiTi components, were evaluated by means of mechanical tests on both coated and uncoated NiTi elements. DMTA provided the evolution of the *tandelta* parameter upon temperature variation and sinusoidal low strains to

assess whether the coating affected the damping ability of the NiTi element. The *tandelta* parameter is related to the dissipative response of the material when subjected to a sinusoidal solicitation: in particular, it represents the ratio between the loss modulus (E'') and the storage modulus (E'), i.e., the out-of-phase and the in-phase response to the sinusoidal solicitation, respectively. The shift in the material's response during the dynamic test is represented by the phase angle δ, and the damping parameter is given by the tan(δ). Figure 5 shows the trends of the *tandelta* for both the uncoated (black line) and coated elements (colored lines). The noise in the curves is due to the instability of the three-point-bending configuration, which does not involve the clamping of the sample's edges. It is possible to observe that in both cases the behavior of the coated and uncoated samples is essentially comparable, since the curves present the same trend and peak intensity in correspondence with the transformations. Moreover, the slight differences that could be observed between some curves (e.g., between Au4N and the other samples in the 0.5 mm thickness group) could be negligible considering the instability and the value fluctuation caused by the experimental conditions of the test.

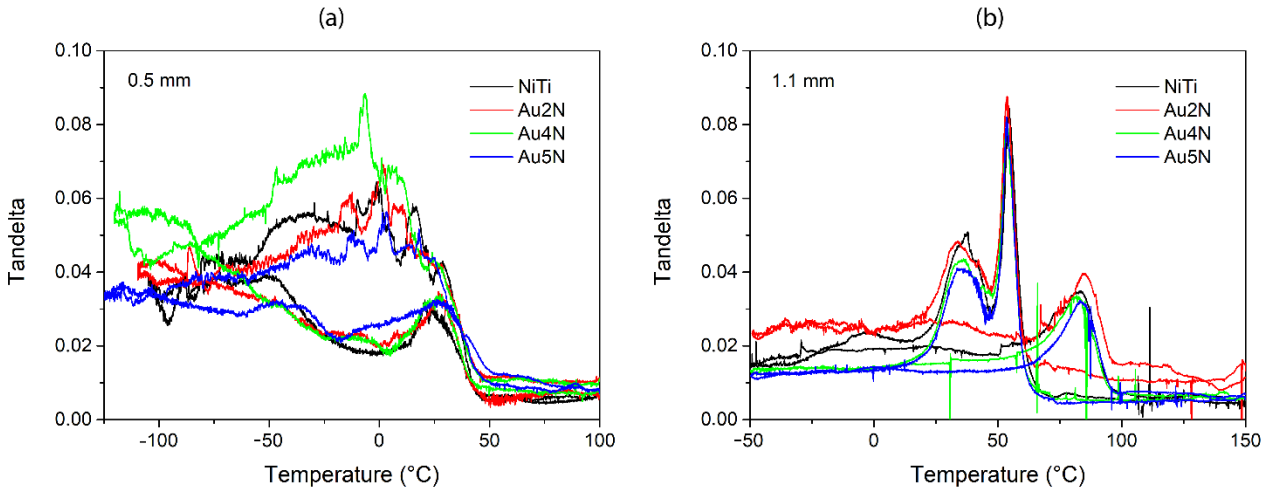

Figure 5. *Tandelta* evolution for coated and uncoated NiTi elements with thickness 0.5 mm (**a**) and 1.1 mm (**b**).

The loading–unloading cycles at high strains allowed the characterization of the pseudoelastic behavior of both coated and uncoated samples. The samples were in austenitic condition (above A_f), and the first cycles allowed the stabilization of the material's response. Then, the typical pseudoelastic behavior upon loading and unloading with hysteresis and without residual strains was observed, even if the signal was quite unstable due to the instability of the three-point-bending loading configuration. In Figure 6, the last cycle for every sample is shown, and the Au-based films evidently provide no significant effect on the flexural behavior of NiTi elements at high strains. Some slight differences were evidenced in the stresses extent for the NiTi substrate in the case of samples with 0.5 mm thickness and for the Au2N coating in the other group. However, in both groups, the different samples have the same trend, approximately the same stresses extent, and completely recover the strain.

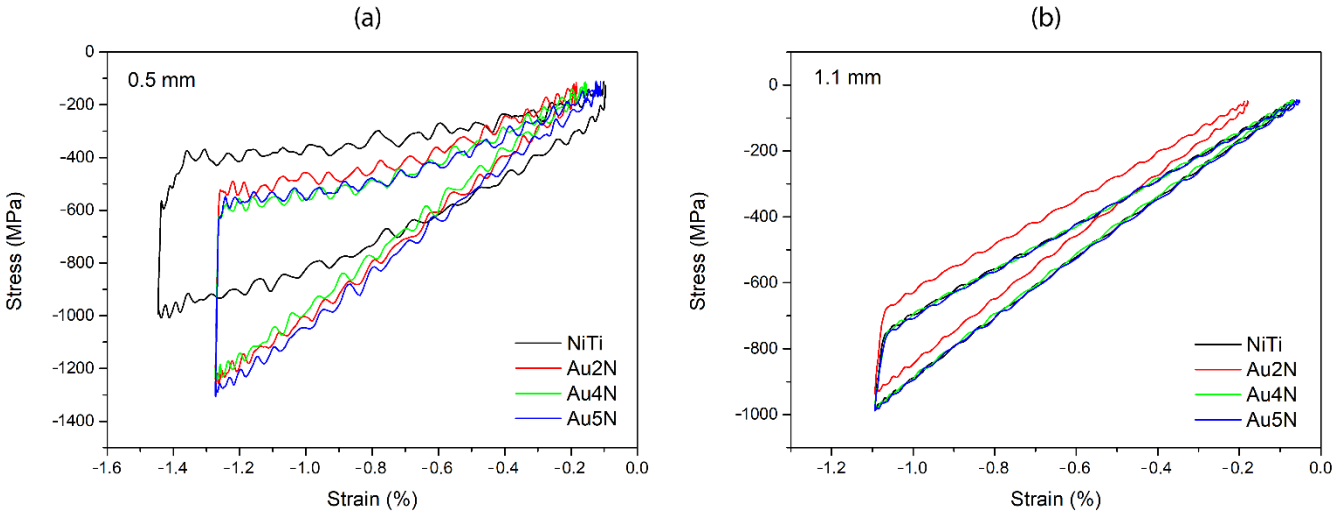

Figure 6. The 1000th loading—unloading cycle for coated and uncoated samples with thickness 0.5 mm (**a**) and 1.1 mm (**b**) in austenitic condition (80 and 120 °C, respectively).

Some qualitative free shape recovery tests (see Figure 7) were performed to investigate the shape-memory ability of the NiTi coated and uncoated elements. The samples were subjected to a severe deformation, and in all cases, the original flat shape was acceptably recovered upon heating to a temperature above A_f.

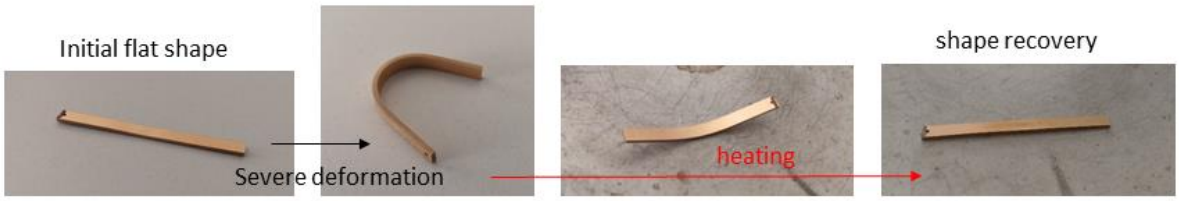

Figure 7. Shape recovery test.

The morphology of the coatings and their adhesion to the substrate after the mechanical tests were evaluated through SEM microscope, and almost no differences were evidenced with respect to the initial film condition. This means that the Au-based film easily accommodates both small and large deformations, indicating a good malleability.

The mechanical characterization of the samples evidenced that the functional properties are not affected by the Au-alloys films, since the functional features and behaviors upon different extents of solicitations of the NiTi elements remains essentially the same. In this way, the potential mechanisms of the SMA component integrated into an accessory, which could exploit one of the functional properties of the SMA itself, would be unchanged. A variation in the SMA response could affect the functioning of a closure or a movement in the accessory, and it could be detrimental. The small thickness of the film is not enough to significantly change the behavior induced not only by large-scale deformations, as evidenced by the cyclic mechanical tests and the free shape recovery tests, but also by small-scale solicitations, as observed in DMTA. The large deformations occurring during pseudoelastic strain of the components or during the shape recovery did not give rise to detachments and removals of portions of the coating, which could have led to the hindrance of the component movement or shape recovery, thereby modifying the functional responses of the whole component. Slight differences between the experimental curves are ascribed to the configurations and to the experimental conditions; hence, the samples behavior could be considered comparable, especially considering the potential application of these coated elements. Indeed, in light of the use of these elements for an ornamental scope, the functional and movement actuation properties are acceptably maintained.

3.3. Mechanical Properties of the Coatings

By stylus profiler analysis, completely comparable roughness values were detected in all samples. The mean roughness (*Ra*) values are around 0.5 µm for both the NiTi substrates and the different coated samples tested. This similarity of values is because the PVD films fully match the morphology of the substrates. Furthermore, the thickness of the coatings (estimated to be in the order of 300 nm, based on the deposition rate of the PVD process) is lower than the average roughness value. A general rule for measuring the mechanical properties of the coating without the contribution of the underlying substrate is to limit the indentation depths to 10% of the coating thickness, thereby ensuring that the elastic–plastic deformation zone is completely contained within the film. Because of the high ratio between sample roughness and film thickness, this rule could not be respected, so it was decided to evaluate the mechanical properties of the entire system constituted by substrate and coating using the CMC loading procedure. In this way, the hardness and reduced modulus are calculated as a function of indentation penetration depth [39]. The trends in both hardness and elastic modulus (Figure 8) are similar in all tested samples: the first 60 nm of displacement, corresponding to about 1/5 of the film thickness, show a considerable increase in both the absolute values of hardness and the data dispersion. Moving from the surface towards the inside of the sample, the curves settle at a plateau whose value is strongly influenced by the substrate properties. The elasticity module decreases more linearly, and a plateau is not as evident as for hardness.

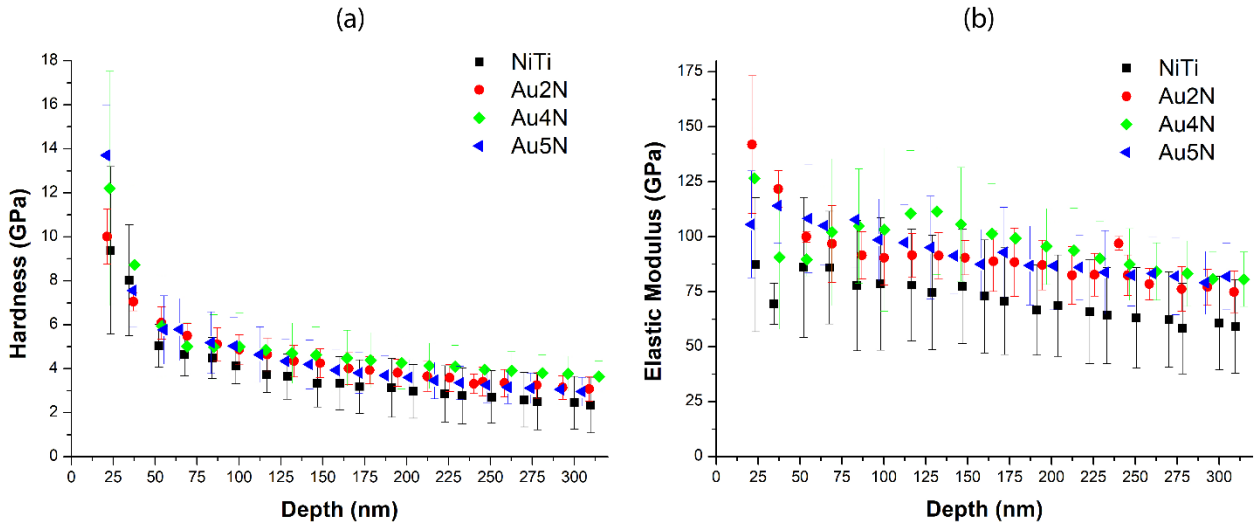

Figure 8. (**a**) Hardness and (**b**) elastic modulus depth profile of gold-alloy-coated samples.

Considering the dispersion of the data, for all coated samples the hardness and elastic modulus values are completely comparable, and on average, they are slightly higher than the corresponding values recorded for the uncoated NiTi substrates.

The adhesion performance of the Au-based coatings on the NiTi substrates is also an essential factor for coating durability. In scratch tests, the critical loads (L_C) are used to evaluate the adhesive strength of a coating/substrate system, which generally can be extrapolated from the acoustic emission (*AE*) signal and friction force curves [40]. These are normally used to evaluate coating cohesion and interfacial adhesion with the substrate. Generally, if the coating is soft, as in this case, significant plastic deformation may be associated with delamination. In Figure 9, friction force, F_x, and acoustic emission as functions of path length are reported for the three Au-based coatings produced in this work.

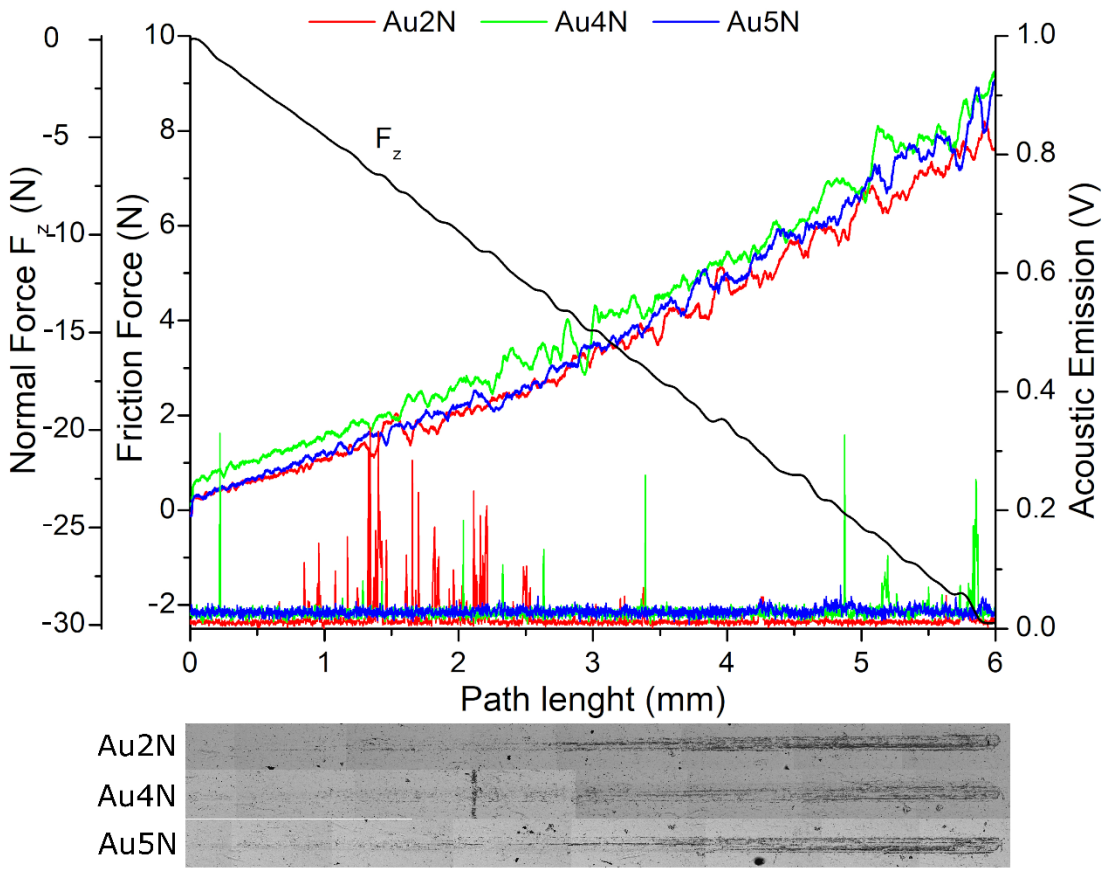

Figure 9. Tribological parameters recorded during scratch tests on Au-base coatings.

All coatings show the typical ductile failure mode without the occurrence of chipping or delamination. The F_x trend is analogue for all the samples. As soon as sliding starts, namely, when the tip is in contact with coating surface at low applied loads, superficial plastic deformation occurs, which is dominated by intrinsic coating properties. In fact, the curve appears a little noisy at first, and reactive force and penetration depth increased linearly with the scratch distance, indicating that plastic deformation occurred in the thin film without cracking it. At about 1.5 mm, which corresponds to an applied normal load of approximately 6 N, a continuous disturbance starts afflicting the F_x curve, thus showing the failure of the material under the tip. This is also visible in the acoustic emission spikes, which are particularly evident for the sample Au2N. The occurrence of structure failure is reflected by the discontinuities that appeared on both measured scratching depth and force. Looking at the electron microscope images of the scratch tracks reported in Figure 9, the beginning of the disturbance on F_x coincides with the first damage to the coatings. In this phase, the plastic deformation advances, and scratch grooves form as the normal load grows progressively. The contact stress increases due to the load concentration in front of the indenter, which is typical of ductile materials. As loading proceeds, material pile-up occurs due to the compressive stress leading to bending of the film. At the same time, radial tensile stresses, due to friction between the indenter and the coating, lead to buckling failures [41,42]. These radial tensile stresses also induce cracks parallel to scratch direction and partial ring cracks, resulting in thorough thickness cracking. This type of failure is characteristic of a ductile failure mode during scratch testing known as conformal cracking. As soon as the friction between indenter and coating increases dramatically, the underlying substrate is exposed, due to breakage of the coating/substrate interface. Figure 10a–c shows details from the scratch tracks on all the tested coatings, where all the described features are clearly visible.

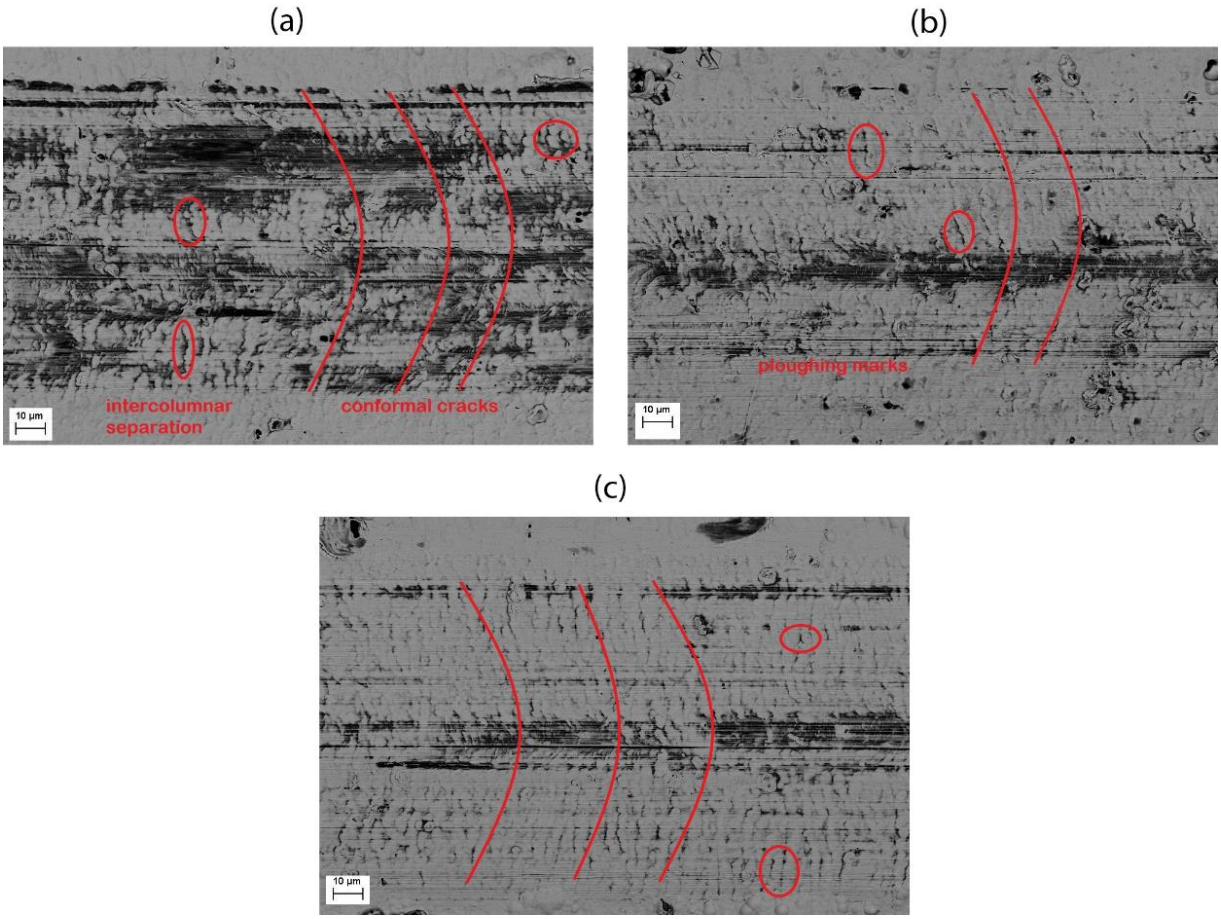

Figure 10. Details of scratch scars for different coatings (**a**) Au2N, (**b**) Au4N, and (**c**) Au5N. Superimposed circles highlight intercolumnar rupture of films.

The intercolumnar separation visible on scratch tracks indicates the cohesive breakdown of the film. The coatings do not undergo brittle break with chipping and delamination, but due to their ductile nature, tend to deform plastically until breakage, resulting from the separation between the columns, which is typical of the microstructure of films obtained via PVD. The presence of conformal cracks, highlighted in Figure 10a–c, and ploughing marks reveal the ductile disruption of the film. Partial exposure of the substrate is visible due to plastic deformation of the substrate too and can be identified with adhesive failure. In any case, the failure of the film is mainly cohesive for all samples, and this allows to positively evaluate the adhesion of all the Au-based films on the substrate of interest. In fact, the mechanical stress produced during the scratch test first causes the film not to break at the interface with the NiTi alloy. Therefore, all the coatings show a satisfactory adhesion on NiTi substrates, and no distinct differences in their adhesive strengths could be observed.

3.4. Wear Tests

Dry wear tests were carried out under atmospheric conditions, resulting in exposure of the substrate due to wear of the grown coatings. Friction coefficient (*COF*) and electric constant resistance (*ECR*) were recorded during sliding test and are reported in Figure 11 for both the coatings and the substrate alone, for comparison.

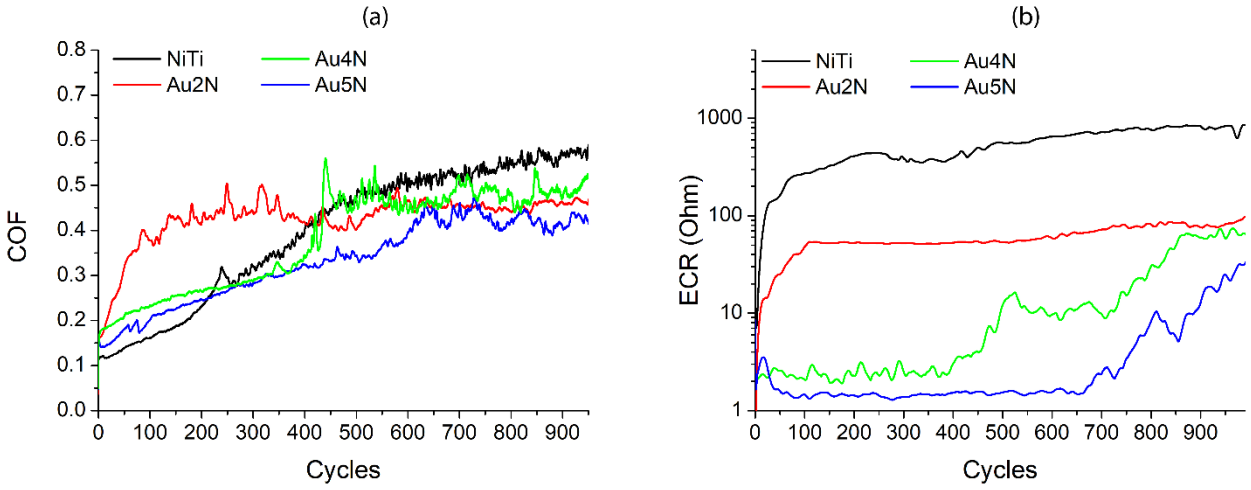

Figure 11. (**a**) Friction coefficient (*COF*) and (**b**) electric constant resistance *(ECR)* during wear tests in dry conditions.

Electric contact resistance is a useful tool to evaluate premature wear [43], since its variation is mainly related to the surface structure, chemistry, contact mechanics, and charge transport mechanisms. In a tribological conductive coupling, wear damages promote the formation of insulating oxide debris, and the consequent *ECR* increase aids in understanding the tribological evolution of the pair. When surface wear and oxide debris are practically nonexistent, a stable and low *ECR* is observed, while the formation of an oxide third body layer, due to wear phenomena, decays the electrical conductance.

From Figure 11a, it appears that friction phenomena occur with the rapid increase in the resisting force opposing the motion of the counterbody on the sample surface. Observing the NiTi substrate curve, initially the growth is steeper, indicating a conditioning of the surface with removal of the protective native oxide layer. In fact, when exposed to air or biological liquids at body temperature, NiTi alloys spontaneously form oxide passive layers [44]. Subsequently a variation of the slope of the curve occurs, suggesting the achievement of a steady state with constant wear rate. The friction coefficient continues to grow due to the increasing roughness in the worn surface.

In all wear tests performed, the coefficient of friction increased quickly to approximately 0.45 for coatings and 0.5 for NiTi substrate at the beginning of the sliding cycles, and then showed a high level of instability during the rest of the experiment. Such instability is likely due to the high levels of contact stress, which causes severe plastic deformation of the sample surface and debris formation thereafter, leading to abrasive wear [45].

For Au-based coatings, the stabilization of *COF* occurs at low level, with a corresponding less severe friction phenomenon, while on NiTi substrate it seems to increase progressively with the number of sliding cycles. Two key factors affect the friction coefficient μ: μ_a, the adhesion force from the atomic interaction between the sliding surfaces and μ_d, which is the force necessary to deform the asperities or plough the surface by the wear debris or asperities [46]. The adhesion contribution μ_a mostly depends on the chemical composition of the two materials in contact, while μ_d is mainly ruled by the yield strength. Since surface mechanical properties of all the samples are very similar, the difference among friction coefficients should be attributed to different chemical composition of the surface. In particular, the Au-based coatings exhibit a lower *COF* at the steady state, and among coatings, the best performing one seems to be the silver-free one, i.e., Au5N. In fact, it reaches the steady state later than the other ones, and its *COF* settles at a slightly lower value.

ECR curves reported in Figure 11b are in good agreement with *COF* trends: in fact, Au4N and Au5N coatings, showing a slower increase in *COF* until the stable state with respect to Au2N, also exhibit the lowest *ECR* values with a progressive escalation. This

means that these Au-based coatings are more resistant to wear phenomena with respect to Au2N sample, for which a rapid increase in *ECR* is observed. The *ECR* rise is related to the formation of an oxide layer at the interface between sliding surfaces, thus revealing that the NiTi substrate is prematurely exposed due to the coating wear. When the noble top layer is progressively worn through and the sliding ball reaches the NiTi substrate, the particles extracted from this non-noble material react with oxygen to form the oxide third body layer, thus increasing *ECR* value [47].

Although there is a rapid increase in *ECR* in Au2N sample, all the coatings reach a stable *ECR* value that is lower than that of the substrate alone, a sign that the coatings are not completely removed during wear tests, thus guaranteeing the electric contact with the sliding sphere. Thanks to its ductile nature and good adhesion to the substrate, the gold-based film accomplishes an effective protective action for the underlying alloy.

3.5. Tribocorrosion Characterization

Tribocorrosion tests performed in Ringer's solution at 37 °C allowed to investigate the behavior of Au-based coatings in simulated body conditions when subjected to rubbing. Both *COF* and *OCV* were recorded during experiments, and curves are reported in Figure 12a,b.

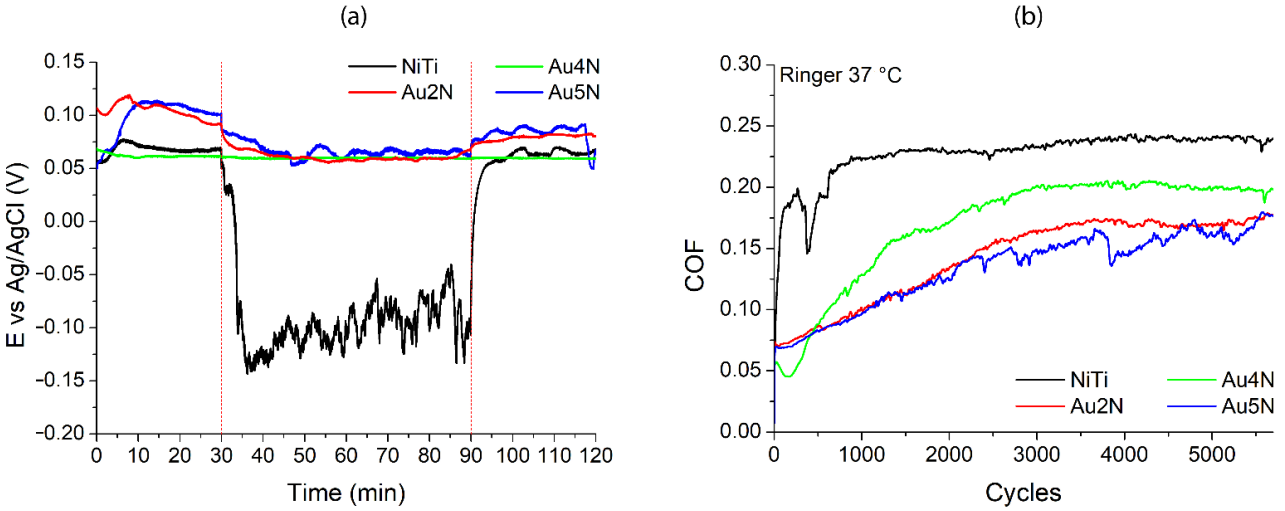

Figure 12. Tribocorrosion parameters, i.e., (**a**) open cell voltage (OCV) during all three phases of test and (**b**) COF during sliding period.

Figure 12a shows the evolution of *OCV* of the contact between ZrO_2- and Au-based coatings or NiTi before, during, and after sliding. The open circuit potential during the sliding process is the result of the combined effect of the potentials of the worn track area and unworn area. Lowering of the open circuit potential is frequently experienced during sliding and wear [48]. The OCV of NiTi abruptly decreases when sliding starts, due to the mechanical detachment of the passive film. It means that the electrochemical activity of freshly exposed surface is higher than the unworn zone. Therefore, the worn area (anode) and the unworn area (cathode) create a galvanic couple due to the potential difference, accelerating the corrosion of the material [49,50]. At each passage, the passive layer is damaged and partially removed, and then immediately restored, in a cyclical process of removal/reformation, which makes the *OCV* trend fluctuate at low nobility values. After the end of the sliding phase, the passivation layer restores and *OCV* returns to initial value in the worn zone. Differently, Au-based coatings exhibit a good protective behavior in Ringer's solution, since *OCV* is little or not at all disturbed during sliding.

Considering instead the *COF* reported in Figure 12b, the NiTi substrate is exposed to a more intense friction phenomenon than that of the coatings, as already observed in the case of dry wear. In the *COF* curves, two friction regimes can be recognized, i.e., a

run-in period, which is characterized by a rapid increase in the measured value of the friction coefficient, followed by a steady-state period. All three films show a transient phase before reaching a stable value for coefficient of friction, which remains lower than the recorded one for the uncoated sample. The increase in *COF* can be attributed to the material wear, which causes particles deliverance, generating ploughing and a third body within the contact zone, thus influencing the tribological pair creating a fast friction transition with increase in *COF* [51,52]. In lubricating conditions, with Ringer's solution as lubricant interposed between the sliding surfaces, sample Au2N and Au5N maintain the lowest *COF*, 0.17, with a very similar trend, while *COF* of 0.2 ad 0.24 are estimated for samples Au4N and NiTi, respectively (see Figure 11b). SEM pictures of tribocorrosion tracks are reported in Figure 13.

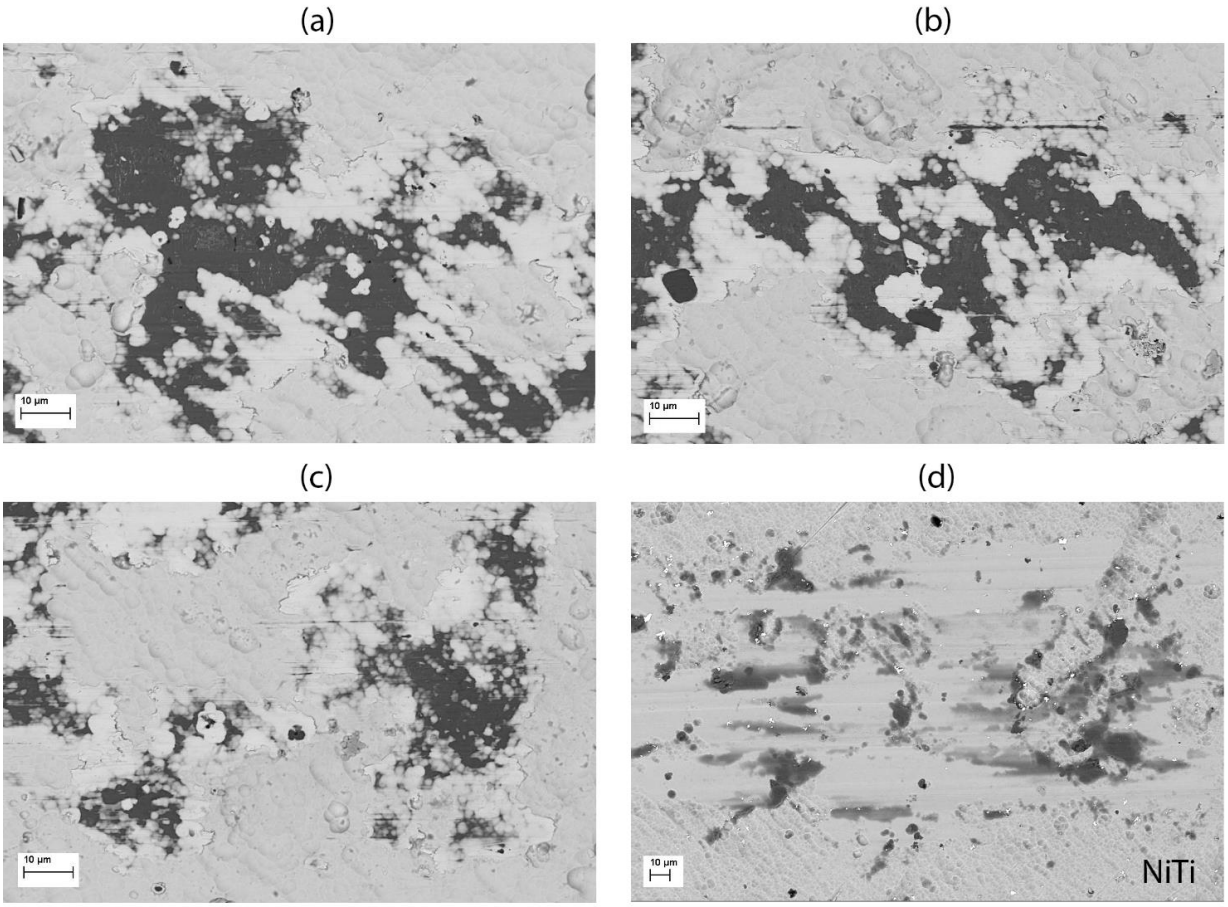

Figure 13. Tribocorrosion tracks on different samples (**a**) Au2N, (**b**) Au4N, (**c**) Au5N, and (**d**) NiTi.

SEM backscattered electron images were collected to evidence differences in chemical composition within the wear scars. Also, X-EDS measurements were carried out to investigate the chemical nature of wear and corrosion products.

Tribocorrosion scars on coated samples show interesting morphological details about wear mode: coatings grains obtained via PVD deposition mode are abraded away during sliding, thus exposing the underlying substrate. Also, in this case, the intercolumnar breakage occurs, together with plastic deformation of coating that is clearly visible around the areas where the substrate is exposed in Figure 13a–c. Within these areas, almost spherical grains are distributed, revealing the internal structure of the coatings: at the film/substrate interface, the coating is not columnar, but it is mainly constituted of small equiaxial grains with a spherical or slightly elongated morphology. No peeling or obvious micro-pores can be detected, though flattened grooves are observed. This indicates that the wear mechanism of the coating is a combination of abrasive wear and plastic deformation [53]. The action of

the ceramic counterbody during the sliding triggers important shear stresses that cause the plastic deformation of the coating material, up to the breaking point of the interface between the columns/grains, with consequent separation and removal of the same.

The ductile behavior of Au-based films is also confirmed by stylus profilometry, as shown in Figure 14, referring to tribocorrosion tracks. While NiTi substrate wears with an irregular topology inside the trace, highlighted by the high roughness that is maintained even after the sliding test, the tribocorrosion traces in the coated samples appear neater and smoother. This is the effect of the plastic deformation of the film, which spreads on the bottom of the track due to the mechanical stress induced by the counterbody. This effect plays an effective role in protecting the underlying material from wear and corrosion and also improves the durability of the deposited coating.

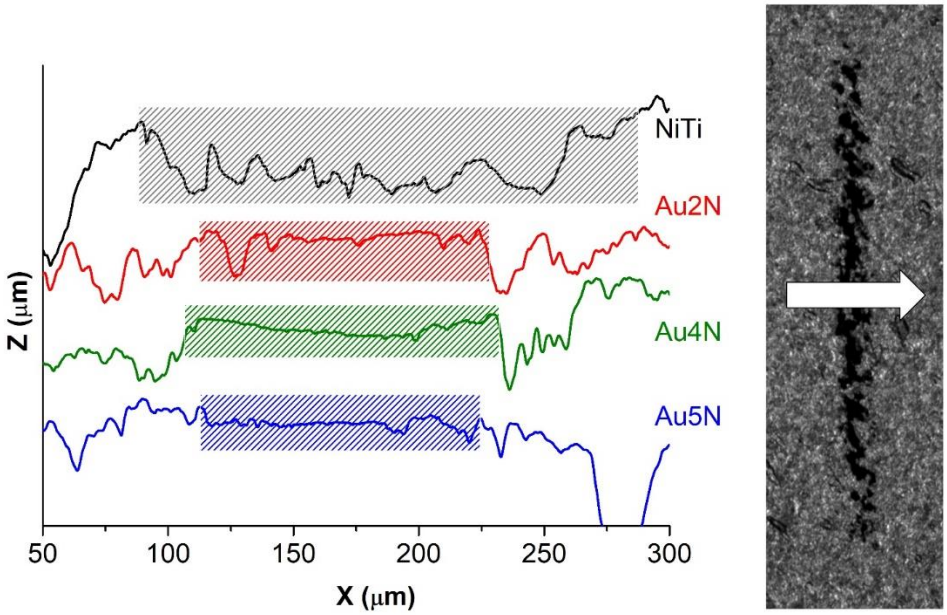

Figure 14. Profiles of tribocorrosion traces, collected transversely to sliding direction.

Considering the noble nature of the coatings, for coated samples the mechanical action of wear is preponderant over the corrosive action of the test medium. The damage mode of the three coatings is identical, while the substrate deviates. Indeed, plastic deformation produced by tangential stresses is not observed, but rather adhesive phenomena are activated with oxidation of the material subjected to wear. Otherwise, for NiTi, the action of the corrosive environment during the mechanical wear plays a noteworthy role due to the good corrosion resistance of this alloy and its ability to passivate through the formation of a protective oxide layer. Mechanical wear exposes the active underlying material by removing its protective layer, and the presence of an oxidizing environment leads to the rapid formation of a new oxide scale, which is again removed by mechanical action and so on. Therefore, in the case of the NiTi alloy, there is a highly synergistic effect between the mechanical action and the aggressive environment, which leads to a faster degradation of the material. The same cannot be said for the noble alloys that constitute the films.

No oxygen signal was found within the tribocorrosion scars on coated sample, while strong oxidation was observed on NiTi. The Zr signal, coming from the counter-body, was not identified in any trace; this is a sign that the material of the ball did not suffer wear during the tests, and consequently, there was no formation of ceramic debris to trigger three-body wear phenomena. Consequently, all the oxygen found inside the wear scars is to be attributed to the oxidation of the NiTi material. The mean width of tribocorrosion scars is different between coated and uncoated samples, while for Au-based coatings it is (85 ± 5) μm for Au2N, (90 ± 5) μm for Au4N, and (83 ± 4) μm for Au5N; in NiTi, the width

of the tribocorrosion track reaches (135 ± 5) μm. The Au-based coating can better resist brittle damage thanks to the ductility and low shear strength of the soft metal phase, which also play a role in lubrication, which reduces the friction coefficient of the coating [54,55]. This can also occur in dry conditions.

Thus, ultimately, all the Au-based coatings characterized in this study proved to be effective in protecting the NiTi substrate, both from wear in dry conditions and in conditions similar to contact with body fluids. The nobility of the materials that compose the films guarantees corrosion protection, and the mechanical wear is mitigated by the ductility of the Au-based alloys and by their ability to deform plastically, which also carries out a lubricating action, thereby lowering the coefficient of friction and the severity of wear.

4. Conclusions

A complete characterization of three Au-based coatings (Au2N, Au4N, and Au5N) deposited by magnetron sputtering on NiTi substrates was performed. The main results are summarized in the following points:

- The deposited films trace and reproduce the substrate surface topology, exhibiting a rough morphology. The obtained colorations, from light yellow to reddish, were in accordance with the indication given by the standards. Moreover, all the Au-based coatings exhibited a microstructural uniformity.
- The first mechanical characterization of the coated NiTi ribbons evidenced that the functional properties were not affected by the application of Au-alloy films, since they could easily accommodate both small and large deformations, indicating good ductility and malleability. Indeed, the damping, shape recovery, and superelastic behavior of the NiTi elements were preserved.
- The evaluation of the mechanical properties of the coating/substrate system was performed using the CMC loading procedure. The evolution of both hardness and elastic modulus values were comparable in all the coated samples, and on average, they were slightly higher than the corresponding values for the uncoated NiTi substrates.
- Scratch tests allowed for the investigation of the adhesion performance of the Au-based coatings on the NiTi substrates and evidenced a ductile failure mode without the occurrence of chipping or delamination. In all cases, the mechanical stress produced during the scratch test did not cause the film break at the interface with the NiTi substrate, but the failure of each film was mainly cohesive, indicating a satisfactory adhesion.
- Both the coefficient of friction (*COF*) and electric contact resistance (*ECR*) were registered during dry wear tests. The two trends were in accordance and indicated that, thanks to their ductile nature and good adhesion to the substrate, all the Au-based films provided an effective protective action for the NiTi component. Indeed, considering the *COF* values, they increased progressively with the number of sliding cycles for the NiTi substrate, while a stabilization trend occurred for the coated samples, indicating a less severe friction phenomenon. Among the coatings, the best performance was given by Au5N, which reached the steady state later than the other ones, and its *COF* settled at a slightly lower value. On the other hand, both Au4N and Au5N coatings, which showed a slower increase in *COF* with respect to Au2N, exhibited the lowest *ECR* plateau, indicating a better resistance to wear.
- Tribocorrosion tests in simulated body fluid allowed the evaluation of the lowering of the open cell voltage (*OCV*), which is frequently observed during sliding and wear in a corrosive environment. The *OCV* of NiTi abruptly decreased when sliding in Ringer's solution started, due to the mechanical detachment of the passive film. In the case of the coated samples, the *OCV* was only slightly disturbed during sliding thanks to the good protective behavior of the Au-coatings in test environment. Moreover, the registered *COF* curves exhibited, as in the dry wear tests, an increasing trend towards a plateau due to the material wear, which generated particle deliverance that induced a lubricating action. This specific wear behavior of the coated samples was confirmed by

the tribocorrosion traces, which appeared smoother thanks to the plastic deformation of the film, therefore protecting the substrate material from wear and corrosion.

The deposited Au-based coatings exhibited good wear resistance in both dry and corrosive conditions, as well as good adhesion, durability, and mechanical properties. Moreover, all the films proved to be effective in protecting the NiTi substrate without affecting its functional and mechanical properties thanks to the ductility of the Au-based alloys and their ability to deform plastically. The behaviors of the three investigated coatings could be considered comparable. Therefore, the variations in the chemistry of deposited films, made to obtain different shades of color, allow to maintain high properties in the final product, satisfying the aesthetic needs of the fashion sector without worsening the behavior of the component during its useful life. Ultimately, by applying these films, not only an aesthetic function is obtained, but also a significant improvement in the mechanical and chemical surface properties of the manufactured articles.

Author Contributions: Conceptualization, F.V., G.d.C., S.V., V.Z., E.M. and E.V.; data curation, F.V.; formal analysis, F.V. and V.Z.; investigation, F.V., E.B., V.Z., E.M., S.M.D. and E.V.; supervision, F.P. and E.V.; visualization, F.V. and V.Z.; writing—original draft, F.V., V.Z., E.M. and E.V.; writing—review and editing, G.d.C. and S.V. All authors have read and agreed to the published version of the manuscript.

Funding: This research received no external funding.

Institutional Review Board Statement: Not applicable.

Informed Consent Statement: Not applicable.

Data Availability Statement: The data that support the findings of this study are available from the corresponding author upon reasonable request.

Acknowledgments: This work was carried out in the framework of INNOSMAD ID546749 Project, PROGRAMMA DI COOPERAZIONE INTERREG V—A ITALIA SVIZZERA CCI 2014TC16RFCB035. The authors are grateful to POSITIVE COATING SA, La Chaux-de-Fonds (CH) for the realization of the Au-based coatings.

Conflicts of Interest: The authors declare no conflict of interest.

References

1. Otsuka, K.; Ren, X. Physical metallurgy of Ti-Ni-based shape-memory alloys. *Prog. Mater. Sci.* **2005**, *50*, 511–678. [CrossRef]
2. Otsuka, K.; Wayman, C.M. *Shape Memory Materials*; Cambridge University Press: Cambridge, UK, 1999.
3. Wolff, I.M. Spangold: A new aura for intermetallics. *Endeavour* **1995**, *19*, 16–19. [CrossRef]
4. Wolff, I.M.; Cortie, M.B. The development of Spangold. *Gold Bull.* **1994**, *27*, 44–54. [CrossRef]
5. Besseghini, S.; Passaretti, F.; Villa, E.; Fabbro, P.; Ricciardi, F. Gold with a martensitic transformation: Which opportunities? *Gold Bull.* **2007**, *40*, 328–335. [CrossRef]
6. Casalena, L.; Coughlin, D.; Yang, F.; Chen, X.; Paranjape, H.; Gao, Y.; Noebe, R.D.; Bigelow, G.S.; Gaydosh, D.J.; Padula, S.A.; et al. Transformation and Deformation Characterization of NiTiHf and NiTiAu High Temperature Shape-memory alloys. *Microsc. Microanal.* **2015**, *21*, 607–608. [CrossRef]
7. Casalena, L.; Bigelow, G.S.; Gao, Y.; Benafan, O.; Noebe, R.D.; Wang, Y.; Mills, M.J. Mechanical behavior and microstructural analysis of NiTi-40Au shape-memory alloys exhibiting work output above 400 °C. *Intermetallics* **2017**, *86*, 33–44. [CrossRef]
8. Beard, G. Jewelry Including Shape Memory Alloy Elements. U.S. Patent 6,675,610 B2, 13 January 2004.
9. Johnson, A.D. TiNi Alloy Company, San Leandro, CA (US), Assignee. Eyeglass Frame. U.S. Patent 7,441,888 B1, 28 October 2008.
10. Beard, G. Manufacturing Method for Jewelry Including Shape Memory Alloy Elements. U.S. Patent 6,910,273 B2, 28 June 2005.
11. Holemans, T.; Stalmans, R. Jewelry Arrangements. E.P. Patent 1 286 606 B1, 1 June 2005.
12. Huynh, K.T. Closure for Article, in Particular for Jewelry. U.S. Patent 2015/0027167 A1, 29 January 2015.
13. Huynh, C. Jewelry That Reversibly Transitions between Two Different Configurations. U.S. Patent 2020/0113296 A1, 16 April 2020.
14. *EN ISO 8654:2018+A1:2019*; Jewellery—Colors of Gold Alloys—Definition, Range of Colors and Designation. Comite Europeen de Normalisation: Brussels, Belgium, 2019.
15. Ahmed, R.A.; Fadl-allah, S.A.; El-Bagoury, N.; El-Rab, S.M.F.G. Improvement of corrosion resistance and antibacterial effect of NiTi orthopedic materials by chitosan and gold nanoparticles. *Appl. Surf. Sci.* **2014**, *292*, 390–399. [CrossRef]
16. Katić, V.; Ćurković, L.; Ujević Bošnjak, M.; Špalj, S. Determination of corrosion rate of orthodontic wires based. *Materialwissenschaft und Werkstofftechnik* **2014**, *45*, 99–105. [CrossRef]

17. Vikulova, E.S.; Karakovskaya, K.I.; Koretskaya, T.P.; Korolkov, I.V.; Chepeleva, E.V.; Asanov, I.P.; Tsygankova, A.R.; Maksimovskii, E.A.; Marchenko, E.S.; Lantsukhay, Y.A.; et al. MOCVD of Noble Metal Film Materials for Medical Implants: Microstructure and Biocompatibility of Ir and Au/Ir Coatings on TiNi. *Coatings* **2021**, *11*, 638. [CrossRef]
18. Es-Souni, M.; Es-Souni, M.; Fischer-Brandies, H. Assessing the biocompatibility of NiTi shape-memory alloys used for medical applications. *Anal. Bioanal. Chem.* **2005**, *381*, 557–567. [CrossRef]
19. Steegmueller, R.; Wagner, C.; Fleckenstein, T.; Schuessler, A. Gold Coating of Nitinol Devices for Medical Applications. *Mater. Sci. Forum* **2002**, *394–395*, 161–164. [CrossRef]
20. Krishnan, M.; Seema, S.; Kumar, A.V.; Varthini, N.P.; Sukumaran, K.; Pawar, V.R.; Arora, V. Corrosion resistance of surface modified nickel titanium archwires. *Angle Orthod.* **2014**, *84*, 358–367. [CrossRef] [PubMed]
21. Gonçalves de Albuquerque, C.; Bortolazzo Correr, A.; Cherubini Venezian, G.; Santamaria, M., Jr.; Tubel, C.A.; Scudeler Vedovello, S.A. Deflection and Flexural Strength Effects on the Roughness of Aesthetic-Coated Orthodontic Wires. *Braz. Dent. J.* **2017**, *28*, 40–45. [CrossRef] [PubMed]
22. Mirvakili, S.M.; Hunter, I.W. Fast Torsional Artificial Muscles from NiTi Twisted Yarns. *ACS Appl Mater. Interfaces* **2017**, *9*, 16321–16326. [CrossRef]
23. Thornton, J.A. High rate thick film growth. *Annu. Rev. Mater. Sci.* **1977**, *7*, 239. [CrossRef]
24. Muller, K.H. Stress and microstructure of sputter-deposited thin films—Molecular dynamics investigation. *J. Appl. Phys.* **1987**, *62*, 1796–1799. [CrossRef]
25. Constantin, R.; Miremad, B. Performance of hard coatings, made by balanced and unbalanced magnetron sputtering, for decorative applications. *Surf. Coat. Technol.* **1999**, *120*, 728–733. [CrossRef]
26. Williams, E.W. Gold ion plating. *Gold Bull.* **1978**, *11*, 30–34. [CrossRef]
27. Oliver, W.C.; Pharr, G.M. An improved technique for determining hardness and elastic modulus using load and displacement sensing indentation experiments. *J. Mater. Res.* **1992**, *7*, 1564–1583. [CrossRef]
28. Oliver, W.C.; Pharr, G.M. Measurement of hardness and elastic modulus by instrumented indentation: Advances in understanding and refinements to methodology. *J. Mater. Res.* **2004**, *19*, 3–20. [CrossRef]
29. *International Standard ISO 20502*; Fine Ceramics (Advanced Ceramics, Advanced Technical Ceramics)—Determination of Adhesion of Ceramic Coating by Scratch Testing. ISO: Geneva, Switzerland, 2007.
30. *ASTM G133-05(2010)*; Standard Test Method for Linearly Reciprocating Ball-on-Flat Sliding Wear. ASTM International: West Conshohocken, PA, USA, 2010.
31. Bushan, B. *Modern Tribology Handbook*; Chapter 3; CRC Press LLC: Boca Raton, FL, USA, 2001.
32. Furko, M.; Balázsi, C. Morphological, Chemical, and Biological Investigation of Ionic Substituted, Pulse Current Deposited Calcium Phosphate Coatings. *Materials* **2020**, *13*, 4690. [CrossRef] [PubMed]
33. Chelliah, N.M.; Padaikathan, P.; Kumar, R. Evaluation of electrochemical impedance and biocorrosion characteristics of as-cast and T4 heat treated AZ91 Mg-alloys in Ringer's solution. *J. Magnes. Alloys* **2019**, *7*, 134–143. [CrossRef]
34. Daniel, R.; Martinschitz, K.J.; Keckes, J.; Mitterer, C. The origin of stresses in magnetron-sputtered thin films with zone T structures. *Acta Mater.* **2010**, *58*, 2621–2633. [CrossRef]
35. Lohmiller, J.; Woo, N.C.; Spolenak, R. Microstructure-property relationship in highly ductile Au-Cu thin films for flexible electronics. *Mater. Sci. Eng. A* **2010**, *527*, 7731–7740. [CrossRef]
36. Michaelsen, C. On the structure and homogeneity of solid solutions: The limits of conventional X-ray diffraction. *Philos. Mag. A.* **1995**, *72*, 813–828. [CrossRef]
37. Liu, J.; Liu, Y.; Gong, P.; Li, Y.; Moore, K.M.; Scanley, E.; Walker, F.; Broadbridge, C.C.; Schroers, J. Combinatorial exploration of color in gold-based alloys. *Gold Bull.* **2015**, *48*, 111–118. [CrossRef]
38. Firstov, G.S.; Vitchev, R.G.; Kumar, H.; Blanpain, B.; Van Humbeeck, J. Surface oxidation of NiTi shape memory alloy. *Biomaterials* **2002**, *23*, 4863–4871. [CrossRef]
39. Saraswati, T.; Sritharan, T.; Mhaisalkar, S.; Breach, C.D.; Wulff, F. Cyclic loading as an extended nanoindentation technique. *Mater. Sci. Eng. A* **2006**, *423*, 14–18. [CrossRef]
40. Steinmann, P.A.; Tardy, Y.; Hintermann, H.E. Adhesion testing by the scratch test method: The influence of intrinsic and extrinsic parameters on the critical load. *Thin Solid Film.* **1987**, *154*, 333–349. [CrossRef]
41. Bull, S.J. Failure modes in scratch adhesion testing. *Surf. Coat. Technol.* **1991**, *50*, 25–32. [CrossRef]
42. Bull, S.J. Failure mode maps in the thin film scratch adhesion test. *Tribol. Int.* **1997**, *30*, 491–498. [CrossRef]
43. Slade, P.G. *Electrical Contacts: Principles and Applications*, 2nd ed.; CRC Press: Boca Raton, FL, USA, 2013.
44. Kosec, T.; Močnik, P.; Mezeg, U.; Legat, A.; Ovsenik, M.; Jenko, M.; Grant, J.T.; Primožič, J. Tribocorrosive Study of New and In Vivo Exposed Nickel Titanium and Stainless Steel Orthodontic Archwires. *Coatings* **2020**, *10*, 230. [CrossRef]
45. Yan, L.; Liu, Y.; Liu, E. Wear behavior of martensitic NiTi shape memory alloy under ball-on-disk sliding tests. *Tribol. Int.* **2013**, *66*, 219–224. [CrossRef]
46. Hutchings, I.M. Friction. In *Tribology, Friction and Wear of Engineering Materials*; Edward Arnold: London, UK, 1992; pp. 22–35.
47. Fouvry, S.; Jedrzejczyk, P.; Chalandon, P. Introduction of an exponential formulation to quantify the electrical endurance of micro-contacts enduring fretting wear: Application to Sn, Ag and Au coatings. *Wear* **2011**, *271*, 1524–1534. [CrossRef]
48. Celis, J.-P.; Ponthiaux, P.; Wenger, F. Tribocorrosion of materials: Interplay between chemical, electrochemical, and mechanical reactivity of surfaces. *Wear* **2006**, *261*, 939–946. [CrossRef]

49. Liu, X.; Zhao, X.; An, Y.; Hou, G.; Li, S.; Deng, W.; Zhou, H.; Chen, J. Effects of loads on corrosion-wear synergism of NiCoCrAlYTa coating in artificial seawater. *Tribol. Int.* **2018**, *118*, 421–431. [CrossRef]
50. Ma, F.; Li, J.; Zeng, Z.; Gao, Y. Tribocorrosion behavior in artificial seawater and anti-microbiologically influenced corrosion properties of TiSiN-Cu coating on F690 steel. *J. Mater. Sci. Technol.* **2019**, *35*, 448–459. [CrossRef]
51. Blau, P.J. On the nature of running-in. *Tribol. Int.* **2005**, *38*, 1007–1012. [CrossRef]
52. Blau, P.J. *Friction Science and Technology*; CRC Press: Boca Raton, FL, USA, 2008; Volume 20084465.
53. Zhang, C.; Farhat, Z.N. Sliding wear of superelastic TiNi alloy. *Wear* **2009**, *267*, 394–400. [CrossRef]
54. Baraket, M.; Mercs, D.; Zhang, Z.G.; Coddet, C. Mechanical and tribological properties of CrN/Ag and CrSiN/Ag nanoscale multilayers. *Surf. Coat. Technol.* **2010**, *204*, 2386–2391. [CrossRef]
55. Cai, K.; Jiang, B.; Zhang, J.; Su, X. Preparation and Tribocorrosion Performance of Different Si-Doped TiSiN-Ag Coatings on Different Substrates in Seawater. *Coatings* **2021**, *11*, 459. [CrossRef]